Research Square

Preprints are preliminary reports that have not undergone peer review.
They should not be considered conclusive, used to inform clinical practice,
or referenced by the media as validated information.

Combining PYROXD2 Overexpression with Anti-PD-1 Immunotherapy Suppresses NSCLC by Promoting NK Cell Infiltration

Li Li
Xuzhou Medical University
Meitao Hu
Xuzhou Medical University
Lixia Zhang
Xuzhou Medical University
Rui Li
Xuzhou Medical University
Zesen Luo
Xuzhou Medical University
Xiaotong Zhou
xtsqzhp@126.com
Xuzhou Medical University

Research Article

Keywords: PYROXD2, Non-small cell lung cancer, NK cell infiltration, PI3K/AKT/mTOR signaling pathway

Posted Date: November 10th, 2026

DOI: https://doi.org/10.21203/rs.3.rs-11457537/v1

License: This work is licensed under a Creative Commons Attribution 4.0 International License.
Read Full License

Additional Declarations: No competing interests reported.

Combining PYROXD2 Overexpression with Anti-PD-1 Immunotherapy Suppresses NSCLC by Promoting NK Cell Infiltration

Li Li[1,2†], Meitao Hu[1,2†], Lixia Zhang[1,2], Rui Li[1,2], Zesen Luo[1,2], Xiaotong Zhou[1,2*]

1. Jiangsu Key Laboratory of Digital Intelligence in Chronic Disease Prevention and Treatment, Thoracic Surgery Laboratory, Xuzhou Medical University, Xuzhou, China;
2. Department of Thoracic Surgery, Affiliated Hospital of Xuzhou Medical University, Xuzhou, China.

[†]Li Li and Meitao Hu contributed equally to this work.
[*]Correspondence: Xiaotong Zhou, Email: xtsqzhp@126.com

Abstract

Background: Non-small cell lung cancer (NSCLC) remains a leading cause of cancer-related mortality. The limited efficacy of current immunotherapies underscores an urgent need for novel therapeutic targets. PYROXD2 has been implicated as a potential tumor suppressor, yet its functional role in NSCLC and the mechanisms by which it modulates the immune microenvironment remain poorly understood.

Methods: Bioinformatics analysis was employed to determine the expression profile and prognostic value of PYROXD2. Its expression in NSCLC tissues and cell lines was validated by qRT-PCR, Western blot, and immunohistochemistry. In vitro and in vivo experiments were conducted; in the in vivo setting, an anti-programmed cell death protein 1 (anti-PD-1) combination treatment was included. Flow cytometry, Transwell co-culture assays, and transcriptome sequencing were utilized to explore its regulatory effects on the tumor microenvironment (TME) and associated signaling pathways.

Results: PYROXD2 was significantly downregulated in NSCLC tissues and cell lines, and its low expression predicted poor prognosis. Both in vitro and in vivo experiments confirmed that PYROXD2 overexpression markedly inhibited the proliferation, migration, and invasion of NSCLC cells and reduced tumor growth in vivo. Mechanistically, PYROXD2 overexpression inhibited the phosphoinositide 3-kinase (PI3K)/AKT/mammalian target of rapamycin (mTOR) signaling pathway, leading to increased interferon-γ (IFN-γ) and decreased tumor necrosis factor-α (TNF-α) levels in tumor tissues, which in turn promoted natural killer (NK) cell infiltration and reduced the accumulation of regulatory T cells (Tregs). Furthermore, anti-PD-1 treatment further enhanced the anti-tumor effect of PYROXD2 overexpression in vivo, as shown by greater tumor growth inhibition in the combination group. Notably, IFN-γ neutralization attenuated NK cell recruitment and partially reversed the anti-tumor effects of PYROXD2, indicating that the PI3K/AKT–IFN-γ–NK cell axis is critical for PYROXD2-mediated tumor suppression.

Conclusion: This study identifies a novel tumor-suppressive function of PYROXD2 in NSCLC

and reveals a key immunomodulatory mechanism, providing a potential combination partner for anti-PD-1 immunotherapy in NSCLC

Keywords: PYROXD2; Non-small cell lung cancer; NK cell infiltration; PI3K/AKT/mTOR signaling pathway

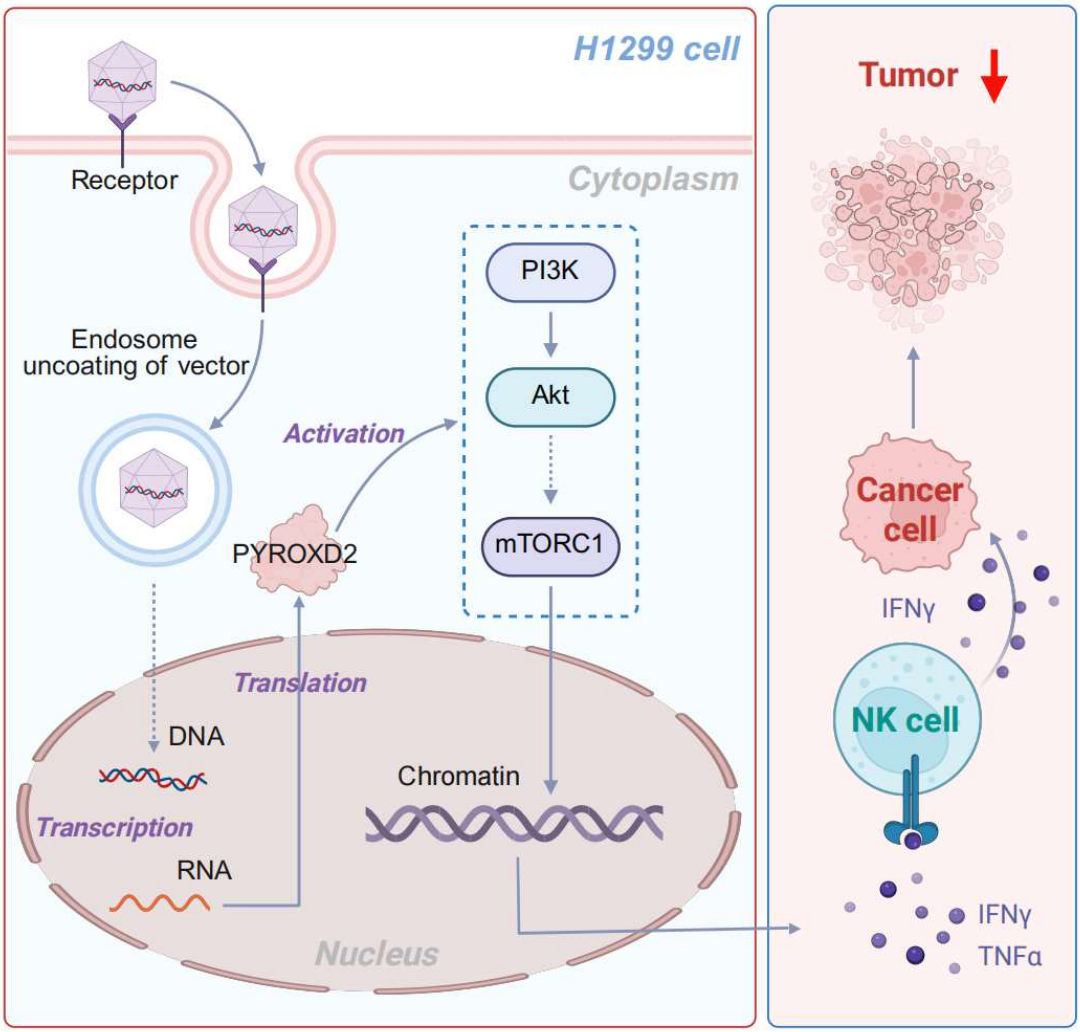
Introduction

Lung cancer remains one of the most common malignancies worldwide and a leading cause of cancer-related mortality, with non-small cell lung cancer (NSCLC) accounting for approximately 85% of cases[1,2]. Despite continuous advancements in surgery, radiotherapy, chemotherapy, and targeted therapies, the 5-year survival rate for patients with advanced NSCLC remains unsatisfactory[3,4]. Immune checkpoint inhibitors (ICIs), particularly PD-1/PD-L1 inhibitors, have provided clinical benefits for a subset of patients by restoring anti-tumor immune activity[5]. However, only about 20–30% of patients achieve durable responses[6-9]. Emerging evidence indicates that the therapeutic efficacy of ICIs is closely associated with alterations in the tumor microenvironment (TME)[10,11]. Insufficient infiltration of effector immune cells, enrichment of immunosuppressive cells, and dysregulation of cytokine networks within the TME can all contribute to tumor immune escape[12-14]. Therefore, elucidating the mechanisms underlying the interaction between cancer cells and the TME is of great significance for improving the efficacy of immune checkpoint blockade (ICB) therapy.

PYROXD2 (pyridine nucleotide-disulphide oxidoreductase domain 2) is a member of the pyridine nucleotide-disulphide oxidoreductase family and plays a crucial role in maintaining mitochondrial redox homeostasis and energy metabolism[15,16]. Previous studies have suggested a potential tumor-suppressive function for *PYROXD2*; for instance, it can induce G1 phase arrest and apoptosis in tumor cells by regulating cell cycle-related proteins[17,18]. Notably, *PYROXD2* is highly expressed in normal tissues but is significantly downregulated in various malignancies, including liver, kidney, bladder cancers, and lung cancer cell lines[19,20], indicating that its loss of expression may play an important role in tumorigenesis and progression. Our preliminary findings further revealed that the expression level of *PYROXD2* is significantly correlated with the infiltration degrees of NK cells and regulatory T cells (Tregs) in NSCLC, implying its potential involvement in TME modulation. However, it remains unclear whether and how *PYROXD2* influences tumor immune surveillance by remodeling the TME. The biological functions and molecular mechanisms of *PYROXD2* in NSCLC progression still lack systematic investigation[20,21].

Therefore, this study aims to systematically elucidate the expression profile and clinical prognostic value of *PYROXD2* in NSCLC, to define its functional role in regulating malignant phenotypes of NSCLC cells such as proliferation, migration, and invasion, and to specifically explore the molecular mechanisms by which it remodels the TME through influencing the infiltration of immune cells like NK cells and Tregs. By integrating multi-dimensional in vitro and in vivo experiments, this research seeks to reveal the core biological significance of *PYROXD2* as a potential tumor suppressor, providing a novel theoretical foundation and experimental basis for

the development of immunotherapeutic targets in NSCLC.



Materials and Methods

Cell Culture and Lentiviral Transfection

Human non-small cell lung cancer (NSCLC) cell lines (H1299, H1975, H23, H226), the human normal bronchial epithelial cell line BEAS-2B, and the mouse Lewis lung carcinoma (LLC) cell line were purchased from Haixing Biosciences (Suzhou, China). H1299, H1975, H23, and H226 cells were cultured in RPMI 1640 medium (Bio-Channel, China) supplemented with 10% fetal bovine serum (FBS; Umedium, China) and 1% penicillin-streptomycin (Bio-Channel, China). BEAS-2B and LLC cells were cultured in DMEM-H medium (Bio-Channel, China) containing 10% FBS and 1% penicillin-streptomycin. All cells were maintained in a humidified incubator at 37 ℃ with 5% CO2.

Lentiviral vectors overexpressing human or mouse *PYROXD2* (*PYROXD2*-OE) and corresponding negative control (NC) vectors were designed and synthesized by GeneChem (Shanghai, China). Cells were transduced with lentivirus using Transfect-Mate transfection reagent (GeneChem) according to the manufacturer's protocol. Subsequently, stably transduced cell populations were selected using 2 μg/mL puromycin (Millipore, USA) for 3-5 days.

All cell lines were authenticated by STR profiling and tested negative for mycoplasma

contamination.

Cell Viability and Proliferation Assays

Cell Counting Kit-8 (CCK-8) Assay: Transfected cells were seeded into 96-well plates at a density of 2×10^3 cells per well. At the indicated time points (0, 24, 48, and 72 h), 10 μL of CCK-8 working solution was added to each well. After 2 hours of incubation, the absorbance at 450 nm was measured using a microplate reader.

Colony Formation Assay: Cells were seeded into 6-well plates at a low density (2,000 cells per well) and cultured in complete medium for 10–14 days. The resulting colonies were washed twice with PBS, fixed with 4% paraformaldehyde for 15 minutes, and stained with 0.1% crystal violet for 20 minutes. After washing and air-drying, colonies containing more than 50 cells were counted manually under a microscope.

EdU Assay: Cell proliferation was detected using the 5-ethynyl-2'-deoxyuridine (EdU) incorporation method with a commercial Click-iT EdU assay kit. Cells were seeded and allowed to adhere. When cell confluence reached approximately 60-70%, EdU was added to the culture medium at a final concentration of 10 μM and incubated at 37 °C for 2 hours. After incubation, cells were fixed with 4% paraformaldehyde at room temperature for 15 minutes and permeabilized with 0.5% Triton X-100 for 10 minutes. Subsequently, a click reaction was performed according to the manufacturer's instructions to covalently conjugate the incorporated EdU with Alexa Fluor 594 azide under light-protected conditions for 30 minutes. Finally, cell nuclei were counterstained with Hoechst 33342. Images were captured using a fluorescence microscope. The proliferation rate was calculated as the percentage of EdU-positive (red fluorescence) cells relative to the total number of Hoechst-positive (blue fluorescence) nuclei in at least five random fields per sample using ImageJ software.

Cell Migration and Invasion Assays

Wound Healing Assay: Cells were seeded into 6-well plates (5×10^5 cells per well) and grown to near confluence. A uniform scratch was created using a sterile 200 μL pipette tip. After washing with PBS to remove detached cells, the cells were incubated in serum-free medium. Images of the wound area were captured at 0 and 24 hours using a phase-contrast microscope. The migration distance was quantified by measuring the change in wound width using ImageJ software.

Transwell Assay: Cell migration and invasion were assessed using 24-well Transwell chambers with 8-μm pore size inserts (Corning, USA). For the invasion assay, the upper chamber membranes were pre-coated with Matrigel (BD Biosciences). Briefly, 2×10^5 cells in serum-free medium were seeded into the upper chamber. The lower chamber was filled with medium containing 10% FBS as a chemoattractant. After 24 hours of incubation, cells that had migrated or invaded to the lower surface of the membrane were fixed with methanol, stained with crystal violet, and counted in five random fields per well under a microscope.

In Vitro Immune Cell Chemotaxis Assay

A co-culture Transwell system was employed to evaluate the chemotactic recruitment of immune cells. *PYROXD2*-OE or control cells (1×10^6 cells/well) were plated in the lower chamber of a 24-well plate. Freshly isolated human peripheral blood mononuclear cells (PBMCs) were then added to the upper chamber. After 24 hours of co-culture, PBMCs that had migrated into the lower

chamber were collected. The cells were stained with a panel of fluorochrome-conjugated antibodies against human immune cell surface markers (including CD45, CD3, CD4, CD8, CD25, CD127, CD19, CD11c, CD16, and CD56; detailed in Table S2). Fluorescence minus one (FMO) controls were used for accurate gating. The stained cells were acquired on a BD LSRII flow cytometer (BD Biosciences, USA) and analyzed using FlowJo software (TreeStar).

RNA Extraction and Quantitative Real-Time PCR (RT-qPCR)

Total RNA was extracted from cultured cells using an RNA Extraction Kit (BGI, Shandong, China). First-strand cDNA was synthesized from 1 μg of total RNA using the HiScript First Strand cDNA Synthesis Kit (BGI, Nanjing, China). Quantitative real-time PCR was performed using the UltraSYBR One-Step RT-qPCR Kit (BGI, Nanjing, China) on a QuantStudio 5 Real-Time PCR System (Applied Biosystems). Gene expression levels were normalized to GAPDH and calculated using the 2^(-ΔΔCt) method. The primer sequences used are listed in Table S2.

Western Blot Analysis

Cells were lysed on ice using RIPA lysis buffer (Sangon Biotech, Shanghai, China). Protein concentrations of the clarified supernatants were determined using a BCA assay. Equal amounts of protein were denatured in loading buffer, separated by SDS-PAGE (80 V for stacking, 120 V for resolving), and subsequently transferred onto methanol-activated PVDF membranes (Millipore, USA) at 300 mA for 60–90 minutes. The membranes were blocked with 5% non-fat milk for 1 hour at room temperature and then incubated overnight at 4°C with the following primary antibodies: anti-*PYROXD2* (1:1000, Abcam), anti-AKT (1:1000, CST), anti-phospho-AKT (Ser473) (1:1000, CST), anti-mTOR (1:5000, Proteintech), anti-phospho-mTOR (Ser2448) (1:2000, Proteintech), and anti-GAPDH (1:50000, Proteintech). After washing with TBST, the membranes were incubated with appropriate HRP-conjugated secondary antibodies (1:5000, ZSGB-BIO, Beijing, China) for 1 hour at room temperature. Protein bands were visualized using an enhanced chemiluminescence (ECL) detection system.

Enzyme-Linked Immunosorbent Assay (ELISA)

Cell culture supernatants were collected and centrifuged to remove debris. The secretion of cytokines (IFN-γ, TNF-α, and IL-12) was quantified using specific ELISA kits (Elabscience, Wuhan, China) according to the manufacturer's instructions. Briefly, 100 μL of supernatant or standard was added to pre-coated wells. After incubation and washing steps, the optical density at 450 nm was measured using a microplate reader.

Flow Cytometry Analysis

For immune cell profiling, single-cell suspensions were prepared from tumor tissues or cultured cells. Approximately 1×10^6 cells were resuspended in PBS containing 2% FBS. The cells were stained with specific fluorochrome-conjugated antibodies (detailed in Supplementary Table S3) on ice for 30 minutes in the dark. After washing, the cells were resuspended in staining buffer and analyzed immediately on a BD LSRII flow cytometer (BD Biosciences, USA). Data were analyzed using FlowJo software (TreeStar).

Multiplex Immunohistochemistry (mIHC)

Formalin-fixed, paraffin-embedded tissue sections (4 μm thick) were deparaffinized and rehydrated. Antigen retrieval was performed in citrate buffer (pH 6.0) using microwave heating. Endogenous peroxidase activity was blocked with 3% H_2O_2. Multiplex staining was performed using a tyramide signal amplification (TSA) kit. Sections were sequentially incubated with a primary antibody, an HRP-conjugated secondary antibody, and a fluorescently labeled tyramide reagent for signal development. This cycle was repeated with different primary antibodies and corresponding fluorophores. Nuclei were counterstained with DAPI. Stained slides were scanned using a multispectral imaging system, and images were analyzed for quantitative assessment of cell populations.

Animal Models and In Vivo Treatments

All animal experiments were conducted in accordance with protocols approved by the Institutional Animal Care and Use Committee of Xuzhou Medical University. Female C57BL/6J mice (5–6 weeks old) were purchased from Cavens Experimental Animal Co., Ltd. (Changzhou, China). For the subcutaneous tumor model, 5×10^5 Lewis lung carcinoma (LLC) cells were injected into the axillary region. For the experimental lung metastasis model, 2×10^5 cells were injected via the tail vein. Tumor dimensions were measured every 4 days using digital calipers, and tumor volume was calculated using the formula: $V = (\text{Length} \times \text{Width}^2) / 2$. For in vivo rescue experiments, mice received intraperitoneal injections of anti-PD-1 antibody (10 mg/kg, clone J43, BioXcell) or anti-IFN-γ antibody every 4 days, starting from day 7 post-tumor inoculation.

RNA Sequencing (RNA-seq) and Bioinformatic Analysis

Total RNA was extracted from H1299-NC and H1299-*PYROXD2*-OE cells using TRIzol reagent. RNA quality was assessed using a NanoDrop 2000 spectrophotometer and an Agilent 2100 Bioanalyzer (RIN > 7.0). Sequencing libraries were constructed using the Illumina TruSeq Kit and sequenced on a NovaSeq 6000 platform (Illumina) with 2×150 bp paired-end reads. Raw sequencing reads were quality-checked with FastQC, trimmed with Trimmomatic, and aligned to the GRCh38 human reference genome using HISAT2. Gene expression levels were quantified as FPKM values using featureCounts. Differentially expressed genes (DEGs) were identified using the DESeq2 package in R, with thresholds set at $|\log_2\text{FoldChange}| > 1$ and an adjusted P-value < 0.05.

Clinical Samples and Database Analysis

Transcriptomic data and corresponding clinical information for NSCLC were downloaded from The Cancer Genome Atlas (TCGA) and the Gene Expression Omnibus (GEO) database (accession GSE103527). The collection and use of human NSCLC tissue samples and adjacent normal tissues were approved by the Ethics Committee of the Affiliated Hospital of Xuzhou Medical University. Written informed consent was obtained from all patients in accordance with the Declaration of Helsinki.

Statistical Analysis

All experiments were performed with at least three independent biological replicates. Data are presented as the mean ± standard deviation (SD). Statistical analyses were performed using GraphPad Prism 8.0 software. Differences between two groups were analyzed using an unpaired,

two-tailed Student's t-test or the Mann-Whitney U test, as appropriate. Survival curves were generated using the Kaplan-Meier method and compared with the log-rank test. A P-value < 0.05 was considered statistically significant.

Results

1. *PYROXD2* is downregulated in NSCLC and predicts unfavorable prognosis

To identify key regulators in the NSCLC tumor immune microenvironment, we performed integrated transcriptomic data analysis. Whole-transcriptome sequencing was conducted on two different types of NSCLC tissues and their adjacent non-cancerous tissues. Joint analysis of the differentially expressed genes from these samples and the GSE103527 immune gene set revealed *PYROXD2* as a significantly downregulated overlapping gene (Fig. 1A). Pan-cancer analysis based on TCGA data further demonstrated that *PYROXD2* mRNA was widely downregulated in various malignancies, including lung adenocarcinoma (LUAD) and lung squamous cell carcinoma (LUSC) (Fig. 1B). Consistent with this, immunohistochemistry (IHC) confirmed that *PYROXD2* protein levels were markedly lower in NSCLC tumor tissues compared to adjacent normal tissues (Fig. 1C). Clinical survival analysis showed that patients with low *PYROXD2* expression had a significantly shorter overall survival (Fig. 1D), establishing its prognostic value. To validate these findings in vitro, we examined *PYROXD2* expression in cell lines. Both RT-qPCR and Western blot analyses confirmed that the mRNA (Fig. 1E) and protein (Fig. 1F, G) levels of *PYROXD2* were significantly downregulated in a panel of NSCLC cell lines (H1299, H23, H226, H1975) compared to the normal bronchial epithelial cell line BEAS-2B. Collectively, these data indicate that *PYROXD2* is a frequently downregulated gene associated with poor overall survival in NSCLC.

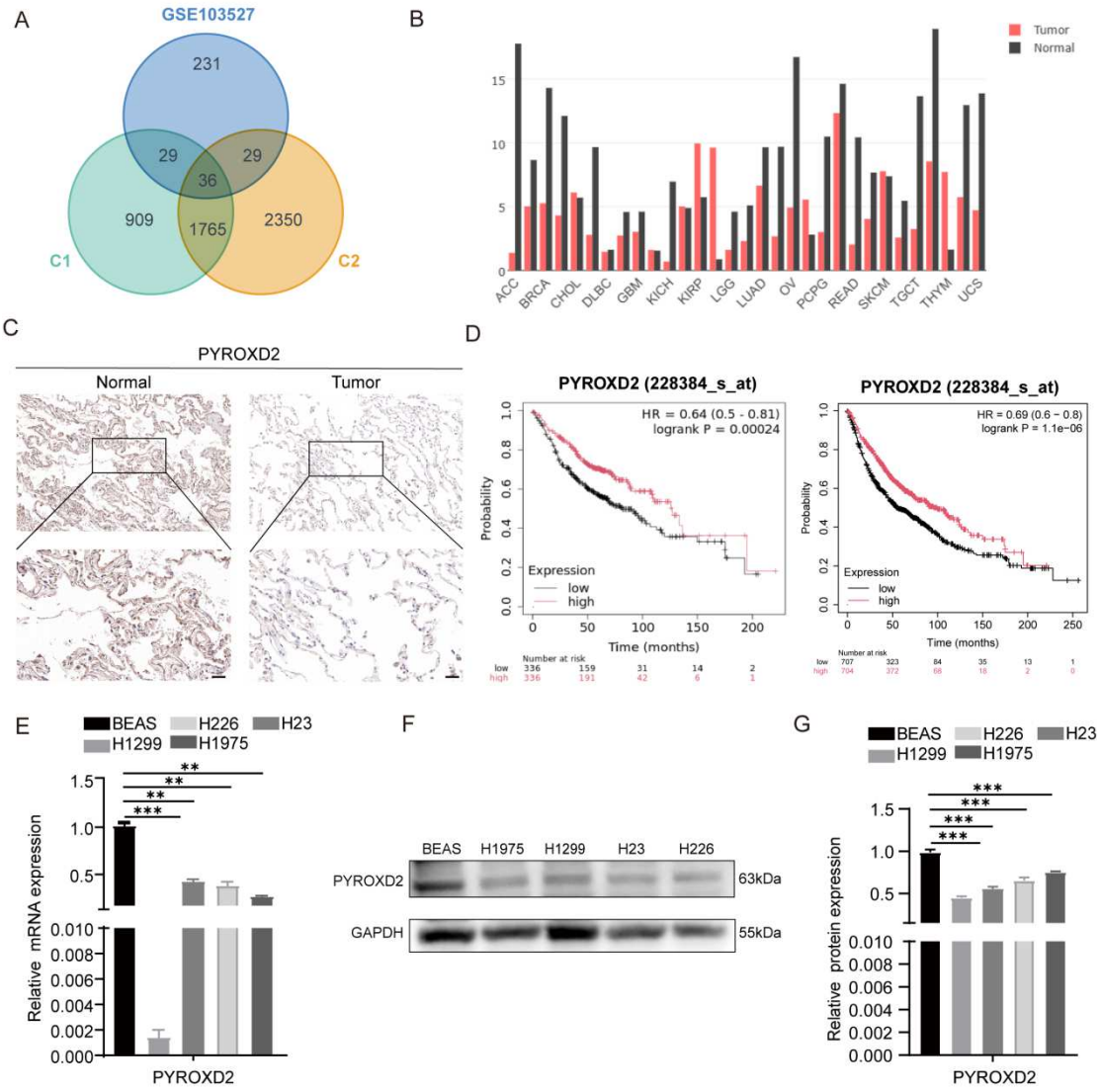


Figure 1. *PYROXD2* is downregulated in NSCLC and correlates with poor prognosis. (A) Venn diagram identifying *PYROXD2* as a commonly downregulated gene from the overlap of differentially expressed genes in two lung cancer samples (C1, C2) and the GSE103527 dataset. **(B)** Pan-cancer analysis of *PYROXD2* mRNA expression (TCGA) shows significant downregulation in multiple cancers including LUAD and LUSC. T: Tumor, N: Normal. **(C)** Representative immunohistochemistry (IHC) staining images of *PYROXD2* in human NSCLC and paired adjacent normal tissues. n=10. Scale bar, 50 μm. **(D)** Kaplan-Meier overall survival curves for NSCLC patients stratified by high vs. low *PYROXD2* expression (log-rank test). **(E)** Relative mRNA expression of *PYROXD2* in a normal bronchial epithelial cell line (BEAS-2B) and NSCLC cell lines measured by RT-qPCR. **(F, G)** Western blot analysis (F) and quantitative densitometry (G) of *PYROXD2* protein expression in the indicated cell lines. GAPDH served as a loading control.Data are presented as mean ± SD. **P < 0.01, ***P < 0.001.

2 *PYROXD2* overexpression suppresses NSCLC cell proliferation in vitro and in vivo

To investigate the functional role of *PYROXD2*, we established stable *PYROXD2*-overexpressing (*PYROXD2*-OE) cell lines using H1299 and H1975 NSCLC cells. Overexpression efficiency was confirmed at both mRNA and protein levels by RT-qPCR and western blot analysis, respectively (Fig. 2A, B). A series of functional assays revealed that *PYROXD2* overexpression significantly impaired the proliferative capacity of NSCLC cells. CCK-8 assay showed reduced cell viability (Fig. 2C). Consistently, EdU incorporation assays demonstrated a marked decrease in DNA synthesis (Fig. 2D, E, H), and colony formation assays confirmed a substantial reduction in long-term clonogenic survival (Fig. 2F, G). To extend these findings to an in vivo setting, we employed a syngeneic subcutaneous tumor model by inoculating C57BL/6J mice with Lewis lung carcinoma (LLC) cells engineered to overexpress *PYROXD2* (Fig. 2I). Mouse body weights remained stable throughout the experiment (Fig. 2J). Tumors derived from *PYROXD2*-OE cells exhibited significantly slower growth kinetics (Fig. 2K) and yielded lower final tumor weights compared to the vector control group (Fig. 2L, M). Immunohistochemical analysis of the excised tumors further revealed a pronounced decrease in Ki67-positive cells within the *PYROXD2*-OE group (Fig. 2N), corroborating the in vitro anti-proliferative effects. Collectively, these data demonstrate that *PYROXD2* functions as a potent inhibitor of NSCLC cell proliferation both in vitro and in vivo.

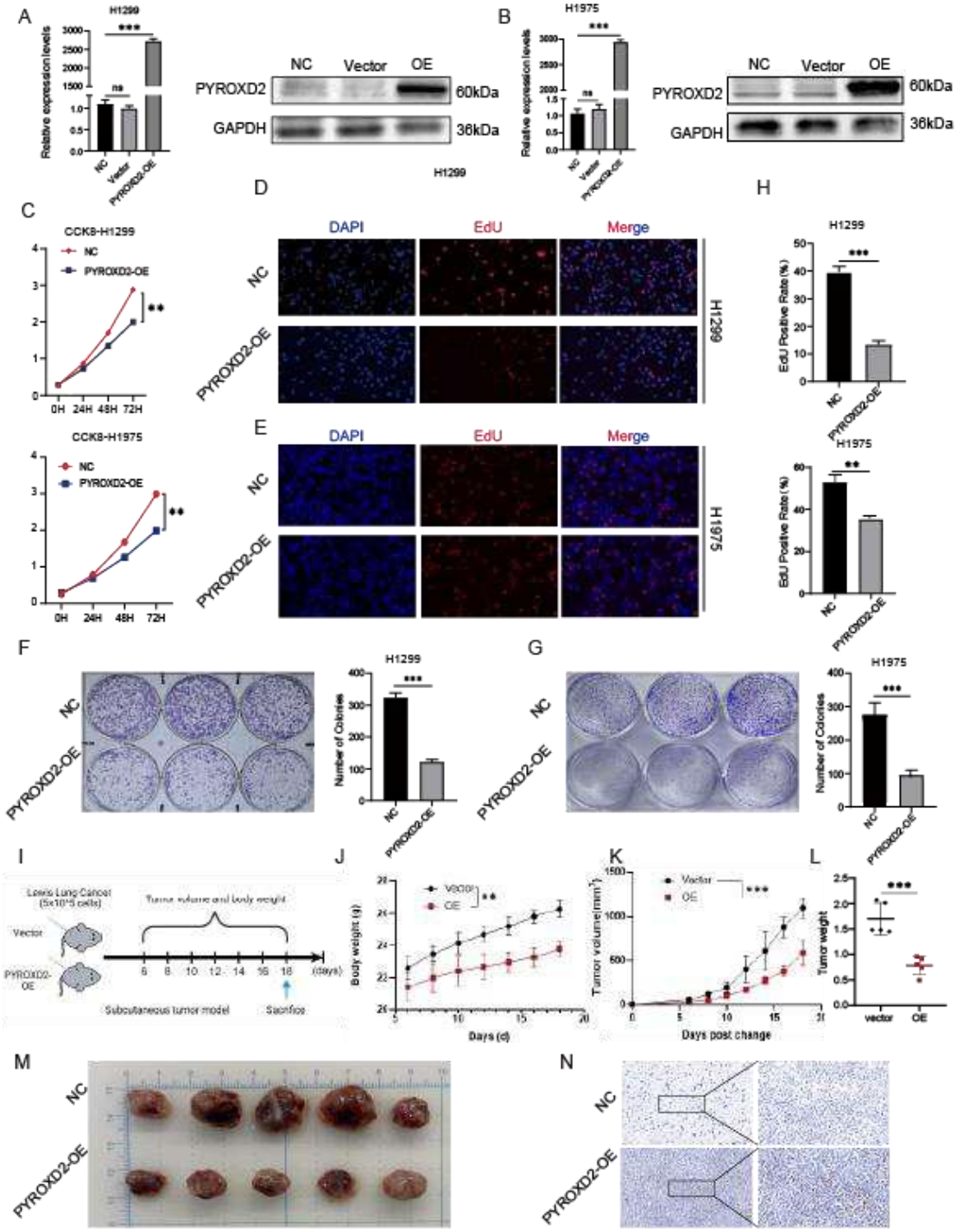


Figure 2. *PYROXD2* overexpression suppresses NSCLC cell proliferation in vitro and in vivo. **(A, B)** Validation of *PYROXD2* overexpression efficiency in H1299 and H1975 cell lines by RT-qPCR (A) and western blot (B). GAPDH served as a loading control. **(C)** Cell viability of H1299 and H1975 cells measured by CCK-8 assay over 72 hours. **(D, E)** Representative fluorescence images from the EdU incorporation assay in H1299 (D) and H1975 (E) cells. EdU

(red) labels proliferating cells; DAPI (blue) stains nuclei. **(F, G)** Representative images (F) and quantitative analysis (G) of colony formation assays for H1299 and H1975 cells. **(H)** Quantitative analysis of EdU-positive cell rates from (D) and (E). **(I)** Schematic of the subcutaneous syngeneic tumor model established with *PYROXD2*-overexpressing or control LLC cells in C57BL/6J mice. **(J)** Body weight curves of mice during the experimental period. **(K)** Tumor growth curves showing volume changes over time. **(L)** Final tumor weights at the experimental endpoint. **(M)** Representative photograph of excised tumors from the Vector and *PYROXD2*-OE groups. n=5. **(N)** Representative immunohistochemistry (IHC) images showing Ki67 expression in xenograft tumor sections. Scale bar, 50 μm.Data are presented as mean ± SD. ns, not significant; **P < 0.01, ***P < 0.001.

3 *PYROXD2* overexpression impairs NSCLC cell migration, invasion, and lung metastasis in vivo

We next investigated the impact of *PYROXD2* on the metastatic potential of NSCLC cells. In vitro functional assays revealed that *PYROXD2* overexpression significantly impaired the migratory and invasive capabilities of H1299 and H1975 cells. Wound healing assays showed a marked delay in wound closure (Fig. 3A, B). Consistently, Transwell assays demonstrated a substantial reduction in both migration (Fig. 3C) and Matrigel invasion (Fig. 3D) upon *PYROXD2* overexpression. To validate these findings in vivo, we established an experimental lung metastasis model by intravenously injecting luciferase-labeled Lewis lung carcinoma (LLC) cells engineered to overexpress *PYROXD2*. In vivo bioluminescence imaging at the experimental endpoint revealed a dramatic attenuation of lung metastasis burden in the *PYROXD2*-OE group, as quantified by relative fluorescence intensity (Fig. 3E, F). Gross examination of excised lungs confirmed that mice bearing *PYROXD2*-OE tumors developed fewer and smaller metastatic nodules compared to the control group (Fig. 3G). Immunohistochemical analysis of lung tissues verified sustained *PYROXD2* expression in metastatic lesions (Fig. 3H) and showed a significant decrease in the proliferation marker Ki67 within the *PYROXD2*-OE group (Fig. 3I). Taken together, these results demonstrate that *PYROXD2* functions as a potent suppressor of NSCLC cell migration, invasion, and distant metastasis.

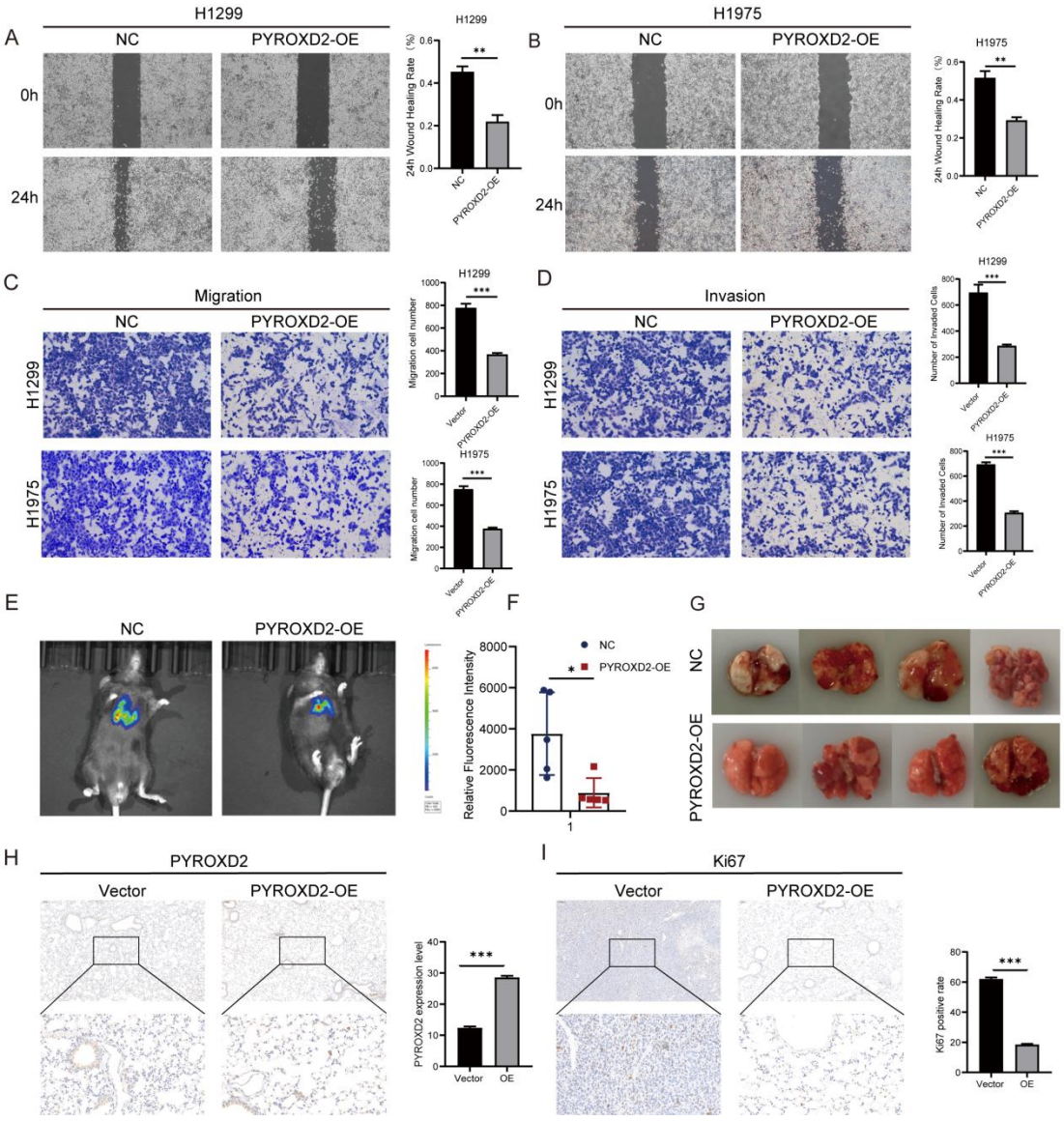


Figure 3. *PYROXD2* overexpression suppresses NSCLC cell migration, invasion, and lung metastasis in vivo. (A, B) Representative phase-contrast images (left) and quantitative analysis (right) of wound healing assays performed with H1299 (A) and H1975 (B) cells transfected with empty vector (NC) or *PYROXD2*-OE plasmids at 0 and 24 hours. **(C)** Representative images (left) and quantification (right) of Transwell migration assays for H1299 and H1975 cells. **(D)** Representative images (left) and quantification (right) of Transwell invasion assays (Matrigel-coated) for H1299 and H1975 cells. **(E)** Representative in vivo bioluminescence images of mice at the experimental endpoint, showing lung metastasis signals. **(F)** Quantification of total flux (relative fluorescence intensity) from the bioluminescence imaging in (E). **(G)** Representative gross photographs of excised lungs from the NC and *PYROXD2*-OE groups. Arrows indicate metastatic nodules. **(H)** Representative immunohistochemistry (IHC) images (left) and quantitative analysis (right) of *PYROXD2* expression in lung metastatic foci. **(I)** Representative IHC images (left) and quantitative analysis (right) of Ki67-positive cells in lung metastatic tissues.Data are presented as mean ± SD. *P < 0.05, **P < 0.01, ***P < 0.001.

4 *PYROXD2* remodels the tumor immune microenvironment by promoting NK cell infiltration

Bioinformatics analysis revealed that in the NSCLC patient cohort, *PYROXD2* expression levels were positively correlated with the enrichment scores of multiple immune-related gene signatures and the stromal score, which assesses stromal cell content (Figures 4A, 4B).

To evaluate the impact of *PYROXD2* overexpression on tumor immune cell infiltration in vivo, flow cytometric analysis was performed on LLC subcutaneous tumor tissues with *PYROXD2* overexpression. The results showed that, compared with the empty vector control group, the proportions of $CD45R^+$ B cells (Figure 4C) and $CD3^+CD8^+$ cytotoxic T cells (Figure 4D) in the *PYROXD2* overexpression group exhibited no significant differences. However, the proportion of infiltrating $NK1.1^+$ NK cells was significantly increased ($P < 0.01$; Figure 4E), while the proportion of $CD25^+FOXP3^+$ regulatory T cells (Tregs) was significantly decreased ($P < 0.01$; Figure 4F). To assess whether *PYROXD2* mediates the chemotactic recruitment of NK cells, Transwell chemotaxis assays were performed in both mouse and human systems. Considering the limited availability of human tumor tissue specimens and and the fact that mouse syngeneic tumors can provide chemotactic sources that more closely mimic the in vivo microenvironment, different methods were used to prepare the chemotactic sources in the two systems. In the mouse system, tissue homogenate supernatants from LLC subcutaneous tumors overexpressing *PYROXD2* or empty vector were used as chemotactic sources and added to the lower chamber of the Transwell. PBMCs isolated from the peripheral blood of C57BL/6J mice were seeded in the upper chamber. After 24 hours of co-culture, the proportion of $NK1.1^+$ cells among the migrated cells in the lower chamber was determined by flow cytometry. The results demonstrated that the tumor homogenate supernatant from the *PYROXD2* overexpression group significantly promoted the migration of mouse $NK1.1^+$ cells ($P < 0.001$; Figure 4G). In the human system, culture supernatants obtained after co-culturing human NSCLC cell line H1299 overexpressing *PYROXD2* or empty vector with human PBMCs for 24 hours were used as chemotactic sources. Fresh human PBMCs were then seeded in the upper chamber of the Transwell. After 24 hours of incubation, the proportion of $CD45^+CD3^-CD56^+$ NK cells among the migrated cells in the lower chamber was measured by flow cytometry. The results showed that the co-culture supernatant from *PYROXD2*-overexpressing H1299 cells and PBMCs significantly promoted the migration of human NK cells ($P < 0.001$; Figure 4H). These results indicate that *PYROXD2* overexpression increases NK cell infiltration and reduces Treg proportions in tumor tissues in vivo, and promotes the directed migration of NK cells in both mouse and human in vitro chemotaxis systems.

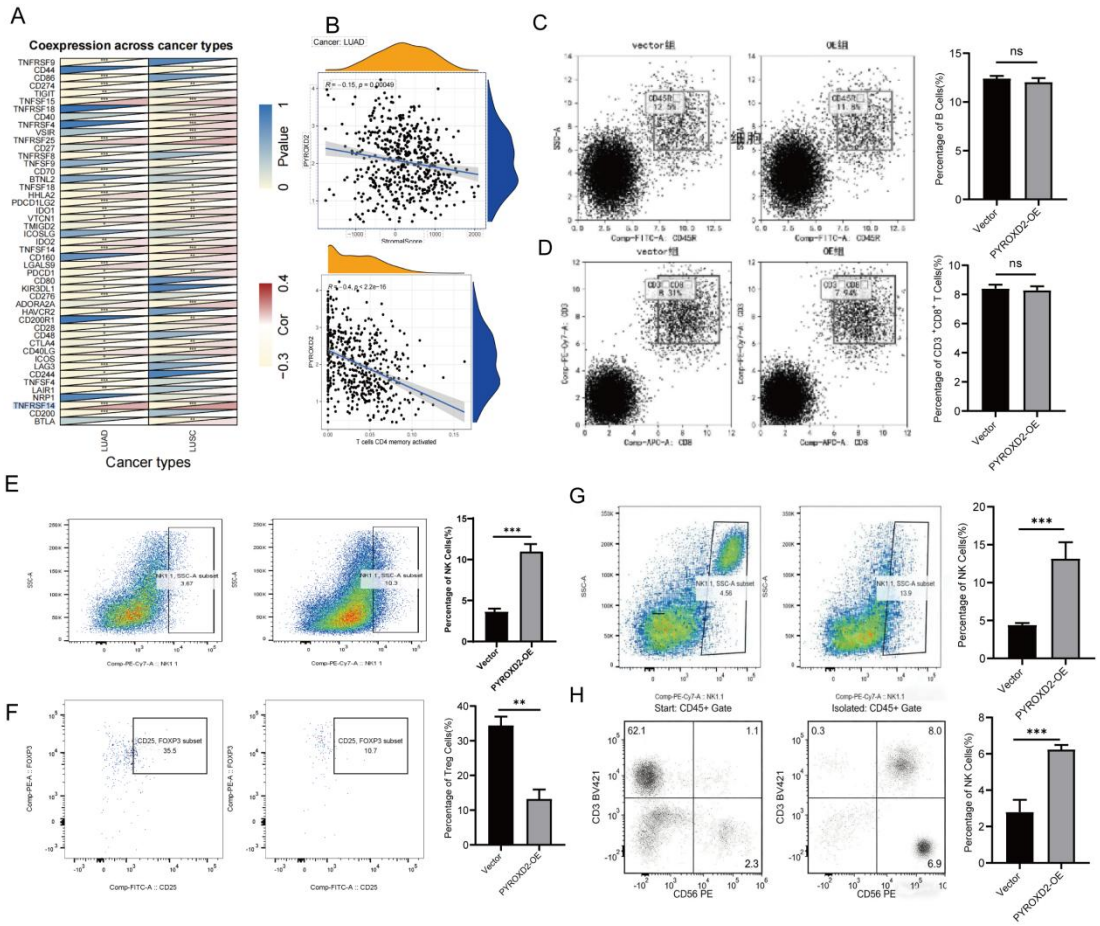


Figure 4. *PYROXD2* remodels the tumor immune microenvironment by promoting NK cell infiltration. (A) Heatmap depicting the correlation between *PYROXD2* expression and immune-related genes in LUAD and LUSC samples from public datasets. **(B)** Scatter plots showing the correlation between *PYROXD2* expression and StromalScore (left) or the infiltration level of activated memory CD4$^+$T cells (right). **(C-F)** Flow cytometric analysis of immune cell populations in subcutaneous xenograft tumors from mice bearing vector control or *PYROXD2*-OE LLC cells. Quantification of (C) CD45R$^+$ B cells, (D) CD3$^+$CD8$^+$ cytotoxic T cells, (E) NK1.1$^+$ NK cells, and (F) CD25$^+$FOXP3$^+$ regulatory T cells (Tregs) .**(G)** Representative flow cytometry plots (left) and quantification (right) of migrated mouse NK1.1$^+$ cells in an in vitro chemotaxis assay co-culturing mouse PBMCs with control or *PYROXD2*-OE LLC cells. **(H)** Representative flow cytometry plots (left) and quantification (right) of migrated human NK cells (gated as CD45$^+$CD3$^-$CD56$^+$) in an in vitro Transwell assay using healthy human PBMCs and H1299 cells.Data are presented as mean ± SD. ns, not significant; **P < 0.01, ***P < 0.001.

5 *PYROXD2* modulates cytokine secretion via suppression of the PI3K/AKT/mTOR signaling pathway

To investigate the molecular mechanisms by which *PYROXD2* regulates the tumor immune microenvironment, transcriptome sequencing (RNA-seq) analysis was performed on H1299 cells with stable *PYROXD2* overexpression and empty vector control cells, identifying a series of differentially expressed genes (Figures 5A, 5C). Gene set enrichment analysis (GSEA) revealed that gene sets associated with the PI3K/AKT signaling pathway were significantly negatively

enriched in the *PYROXD2* overexpression group (Figure 5B). Gene Ontology (GO) and Kyoto Encyclopedia of Genes and Genomes (KEGG) pathway enrichment analyses based on these differentially expressed genes further corroborated this finding (Figure 5D).

Western blot results showed that the phosphorylation levels of AKT (Ser473) and mTOR (Ser2448) were significantly reduced in *PYROXD2*-overexpressing cells, while the total protein levels of both remained unchanged ($P < 0.05$ and $P < 0.01$; Figures 5E, 5F).ELISA results demonstrated that in the tumor tissue homogenate supernatant of the *PYROXD2* overexpression group, IFN-γ levels were significantly increased, while TNF-α levels were significantly decreased ($P < 0.001$; Figure 5G). Following treatment with the mTOR inhibitor rapamycin (100 nM, 24 h), mTOR phosphorylation levels in *PYROXD2*-overexpressing cells were further decreased ($P < 0.001$; Figure 5H).Treatment with the mTOR inhibitor rapamycin (100 nM, 24 h) further decreased mTOR phosphorylation but did not enhance IFN-γ production; instead, it partially reversed PYROXD2-induced IFN-γ upregulation (Figure 5H, I). These results suggest that the PI3K/AKT/mTOR pathway is involved in PYROXD2-mediated IFN-γ regulation, but mTOR may not be the sole downstream mediator; PI3K/AKT may act through alternative effectors such as FOXO transcription factors. Collectively, PYROXD2 overexpression suppresses PI3K/AKT/mTOR signaling and promotes IFN-γ secretion, and that the PI3K/AKT pathway may regulate IFN-γ through downstream effectors other than mTOR, such as FOXO transcription factors. overexpression suppresses the activity of the PI3K/AKT/mTOR pathway and promotes IFN-γ secretion. The partial reversal effect of rapamycin suggests that the PI3K/AKT/mTOR pathway at least partially mediates the regulation of IFN-γ secretion by *PYROXD2*.

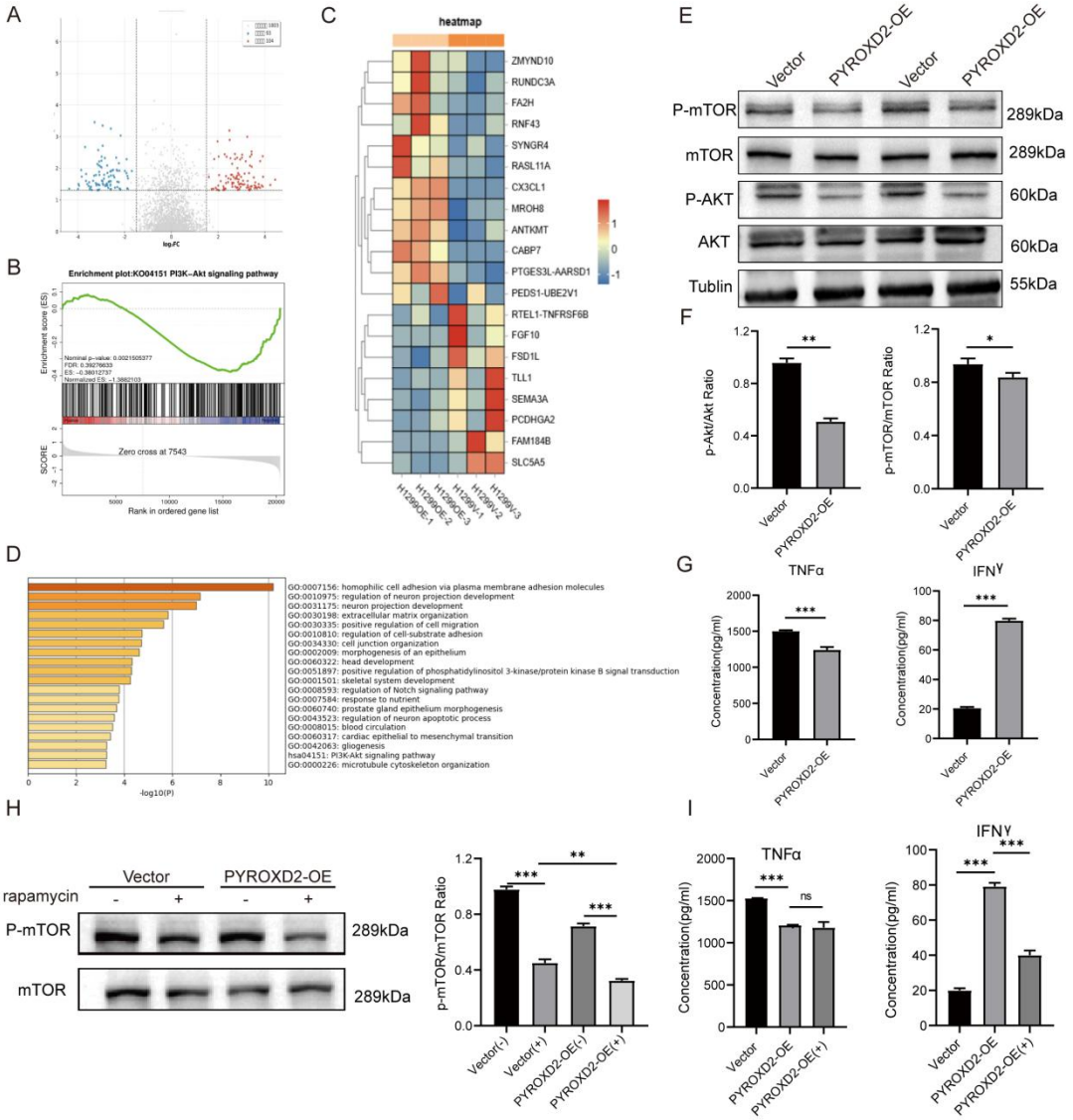


Figure 5. *PYROXD2* regulates cytokine secretion by inhibiting the PI3K/AKT/mTOR pathway. (A) Volcano plot of differentially expressed genes (DEGs) between Vector and *PYROXD2*-OE H1299 cells from RNA-seq data ($|\log_2 FoldChange| > 1$, $P < 0.05$). **(B)** Gene Set Enrichment Analysis (GSEA) plot showing significant negative enrichment of the PI3K/AKT signaling pathway gene set in *PYROXD2*-OE cells. **(C)** Heatmap of hierarchical clustering for representative DEGs. **(D)** Bar chart of the top enriched KEGG pathways and Gene Ontology (GO) biological processes for the identified DEGs. **(E)** Western blot analysis of phosphorylated and total levels of AKT and mTOR in the indicated cell lines. β-Tubulin served as a loading control. **(F)** Quantification of the p-AKT/AKT and p-mTOR/mTOR ratios from (E). **(G)** Concentrations of TNF-α and IFN-γ in cell culture supernatants measured by ELISA. **(H)** Western blot analysis (left) and quantification (right) of p-mTOR/mTOR ratios in cells treated with or without the mTOR inhibitor Rapamycin (100 nM, 24 h). **(I)** ELISA quantification of TNF-α and IFN-γ levels in supernatants from cells with the indicated treatments (+/- Rapamycin).Data are presented as mean ± SD. ns, not significant; *P < 0.05, **P < 0.01, ***P < 0.001.

6 *PYROXD2* orchestrates a PI3K/AKT-IFN-γ signaling loop to recruit NK cells and suppress

tumor progression in vivo

To establish the functional importance of the PI3K/AKT-IFN-γ axis identified in Figure 5, we performed in vivo rescue experiments in mice bearing *PYROXD2*-overexpressing tumors. Mice were treated with neutralizing antibodies against IFN-γ or PD-1 (Fig. 6A). Bioluminescence imaging revealed that blockade of IFN-γ significantly rescued the tumor-suppressive phenotype induced by *PYROXD2* overexpression, leading to increased tumor burden (Fig. 6A, C). In contrast, anti-PD-1 treatment further inhibited tumor growth in PYROXD2-overexpressing tumors compared with the isotype control (Fig. 6A, C). Analysis of the tumor immune microenvironment showed that anti-IFN-γ treatment markedly attenuated the *PYROXD2*-driven accumulation of tumor-infiltrating NK cells ($CD3^{-}NK1.1^{+}$), as assessed by both flow cytometry (Fig. 6B, D) and immunohistochemistry (Fig. 6E, F). Conversely, PD-1 blockade further enhanced NK cell infiltration in the *PYROXD2*-OE context (Fig. 6B, D-F). These data demonstrate that IFN-γ is a critical downstream effector mediating the anti-tumor and immunomodulatory functions of *PYROXD2*, and they delineate a positive regulatory loop wherein *PYROXD2*, via inhibiting PI3K/AKT signaling, promotes IFN-γ secretion to recruit NK cells, ultimately suppressing NSCLC progression.

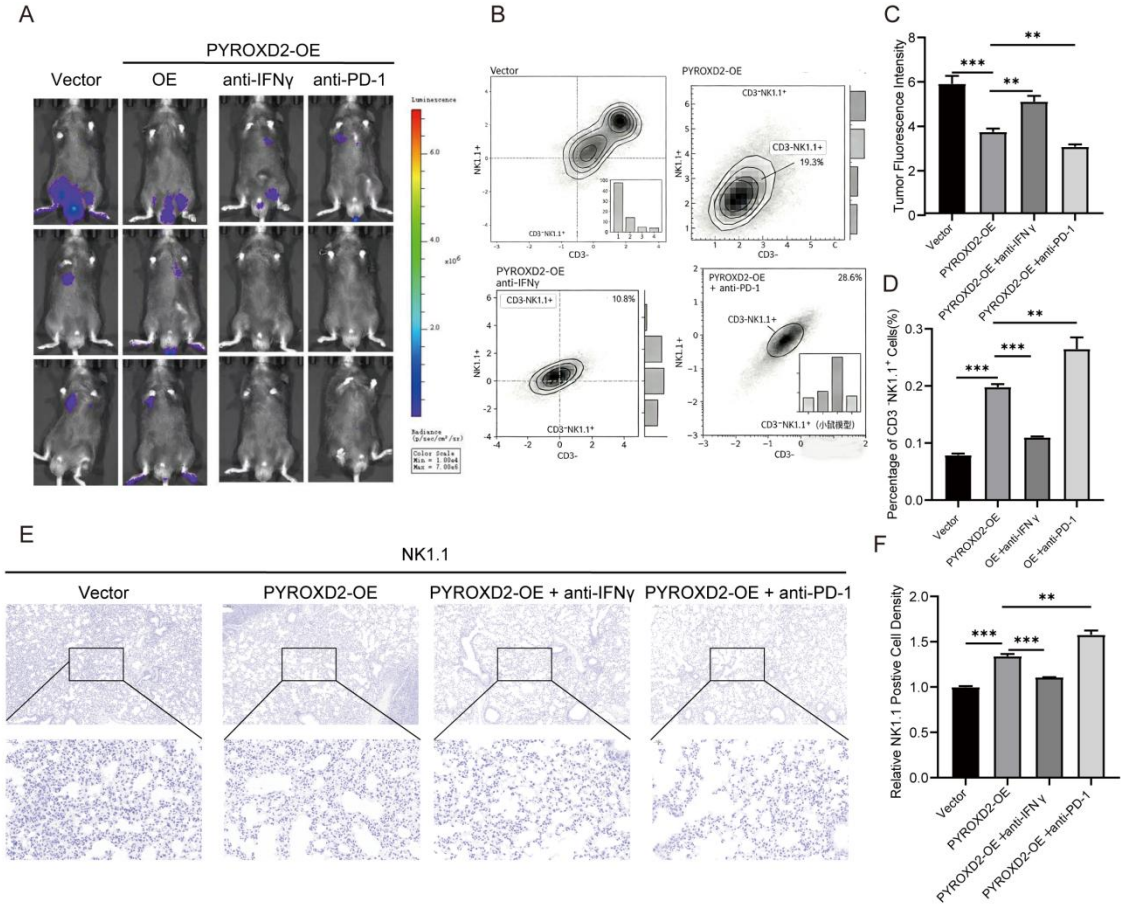


Figure 6. *PYROXD2* recruits NK cells via a PI3K/AKT-IFN-γ signaling loop to inhibit tumor progression in vivo. (A) Representative in vivo bioluminescence images of mice bearing Vector control or *PYROXD2*-overexpressing (*PYROXD2*-OE) LLC tumors, treated with isotype control, anti-IFN-γ, or anti-PD-1 neutralizing antibodies as indicated. **(B)** Representative flow cytometry contour plots showing the gating strategy for tumor-infiltrating NK cells ($CD3^{-}NK1.1^{+}$) from dissociated tumors in each treatment group. **(C)** Quantification of total tumor bioluminescence

flux (radiance) from the images in (A). **(D)** Quantitative analysis of the percentage of $CD3^{-}NK1.1^{+}$ NK cells among live $CD45^{+}$ leukocytes from flow cytometry data in (B). **(E)** Representative immunohistochemistry (IHC) images of NK1.1 staining in excised tumor sections from the indicated groups. Scale bar, 50 μm. **(F)** Quantification of NK1.1-positive cell density per field from IHC analysis in (E).Data are presented as mean ± SD. $^{**}P < 0.01$, $^{***}P < 0.001$.

Discussion

In this study, we identify *PYROXD2* as a novel tumor suppressor in non-small cell lung cancer (NSCLC). Integrated analyses of clinical cohorts and transcriptomic data revealed that *PYROXD2* is frequently downregulated in NSCLC tissues, and its low expression correlates with unfavorable patient prognosis[23,24]. Functionally, restoring *PYROXD2* expression potently inhibited NSCLC cell proliferation, migration, and metastasis in vitro and in vivo. More importantly, we uncovered a previously unrecognized immunomodulatory role of *PYROXD2*: it reprograms the tumor immune microenvironment (TIME) by suppressing the PI3K/AKT signaling pathway[46,47], thereby augmenting IFN-γ secretion and subsequent natural killer (NK) cell recruitment[25-27,49]. These findings not only redefine *PYROXD2* as a critical nexus between tumor-intrinsic signaling and anti-tumor immunity but also provide a rationale for combining *PYROXD2*-based therapy with immune checkpoint blockade.

Previous investigations into *PYROXD2* have primarily centered on its intracellular functions in redox homeostasis and stress response. For instance, PYROXD2 has been characterized as a thioredoxin-like enzyme[15]. Ribosomal protein L3 (RPL3) has been implicated in translation fidelity under metabolic stress[28]. Similarly, studies in congenital myopathy models have linked PYROXD2 deficiency to exacerbated protein aggregation and oxidative damage, underscoring its role in maintaining cellular redox balance[29]. However, these reports were confined to cell-autonomous processes, leaving its potential impact on the broader tumor ecosystem—particularly the immune landscape—completely unexplored. Our work bridges this critical gap by shifting the paradigm of *PYROXD2* from a metabolic regulator to a potent immunomodulator, demonstrating its capacity to shape a permissive TIME in NSCLC.

A key advance of our study is the elucidation of the crosstalk between *PYROXD2* and innate immunity, specifically NK cells. While adaptive immune checkpoints (PD-1/PD-L1) have dominated cancer immunotherapy[30], the antigen-independent cytotoxicity of NK cells offers a promising alternative, especially in immunologically “cold” tumors[31]. Nonetheless, NK cells are often functionally impaired or excluded within immunosuppressive microenvironments[32], and their anti-tumor function is intricately linked to metabolic state[48]. Through RNA sequencing and functional validation, we found that *PYROXD2* overexpression robustly inhibits the PI3K/AKT pathway[33], a central oncogenic driver across many cancers[47]. Mechanistically, attenuation of PI3K/AKT signaling is known to promote FOXO1 nuclear translocation, which relieves transcriptional repression of IFNG and enhances IFN-γ production[34,35]. Consistent with this paradigm, we observed that *PYROXD2*-mediated PI3K/AKT suppression led to a marked increase in IFN-γ secretion. This cytokine surge effectively recruited and activated NK cells into the tumor bed[36,37], which in turn can produce additional IFN-γ, establishing a self-amplifying positive

feedback loop that sustains and amplifies anti-tumor immunity[36].

Our in vivo rescue and combination experiments further underscore the translational relevance of this axis. Neutralizing IFN-γ largely abrogated the *PYROXD2*-driven NK cell infiltration and partially reversed tumor suppression, establishing a causal link within the *PYROXD2*–PI3K/AKT–IFN-γ–NK cell circuit. Notably, combining PYROXD2 overexpression with PD-1 blockade further enhanced the anti-tumor effect and NK cell recruitment compared with PYROXD2 overexpression alone, delaying tumor progression. This finding has clinical implications, as many NSCLC patients exhibit primary resistance to immune checkpoint blockade due to an immune-desert or excluded tumor phenotype, a process shaped by tumor immunoediting and various resistance mechanisms[39,40,38,50,51].Strategies to elevate PYROXD2 expression may therefore serve as a viable approach to convert “cold” tumors into “hot,” immunologically active ones, potentially improving their responsiveness to existing immunotherapies.[41,42].

Despite these insights, our study has limitations that warrant future investigation. First, the precise molecular mechanism by which *PYROXD2* directly interacts with upstream components to inactivate the PI3K/AKT pathway remains unclear; detailed biochemical studies (e.g., co-immunoprecipitation, mass spectrometry) are needed to identify binding partners. Second, while we used immunocompetent murine models, humanized mouse systems would better recapitulate human immune cell interactions and facilitate the preclinical evaluation of *PYROXD2*-targeted strategies[43].

In conclusion, our study unveils a novel tumor-suppressive and immunomodulatory role for *PYROXD2* in NSCLC. We demonstrate that *PYROXD2* operates through the PI3K/AKT–IFN-γ–NK cell axis to restrict tumor progression and remodel the TIME. These findings expand the functional repertoire of *PYROXD2* beyond metabolism and provide a compelling rationale for developing combination therapies that leverage NK cell engagement[44,45] alongside conventional immune checkpoint inhibition, potentially by targeting co-inhibitory receptors like TIGIT[52], which is expressed on both NK cells and T cells.

Author contributions:
Li Li: Methodology, Formal analysis, Writing – original draft.
Meitao Hu: Validation, Investigation.
Lixia Zhang: Investigation, Data curation.
Rui Li: Resources, Validation.
Zesen Luo: Software, Visualization.
Xiaotong Zhou: Conceptualization, Supervision, Writing – review & editing.

Funding: This work was supported by the Postgraduate Research & Practice Innovation Program of Jiangsu Province (Grant No. KYCX25_3299).

Data availability: The raw data supporting the conclusions of this article will be made available by the corresponding author upon reasonable request. No unique reagents were generated in this study.

Conflict of interest The authors declare no competing interests.

Ethical approval The requirement for informed consent was waived by the Ethics Committee of the Affiliated Hospital of Xuzhou Medical University (XYFY2022-KLi35-02). This study was conducted in accordance with the Declaration of Helsinki. The requirement for informed consent was waived by the Ethics Committee of the AffiliatedHospital of Xuzhou Medical University. All animal experiments were conducted in accordance with protocols approved by the Institutional Animal Care and Use Committee of Xuzhou Medical University (Approval No. 202412T006).

References

1. Bray F, Laversanne M, Sung H, et al. Global cancer statistics 2022: GLOBOCAN estimates of incidence and mortality worldwide for 36 cancers in 185 countries. CA Cancer J Clin. 2024;74(3):229-263.
2. Sung H, Ferlay J, Siegel RL, et al. Global Cancer Statistics 2020: GLOBOCAN Estimates of Incidence and Mortality Worldwide for 36 Cancers in 185 Countries. CA Cancer J Clin. 2021;71(3):209-249.
3. Howlader N, Forjaz G, Mooradian MJ, et al. The Effect of Advances in Lung-Cancer Treatment on Population Mortality. N Engl J Med. 2020;383(7):640-649.
4. Herbst RS, Morgensztern D, Boshoff C. The biology and management of non-small cell lung cancer. Nature. 2018;553(7689):446-454.
5. Zecevic A, Blanka-Protic A, Jandric A, et al. Are patients with chronic obstructive pulmonary disease at a greater risk for the development of autoimmune thyroiditis as an adverse event of immunotherapy in non-small cell lung cancer treatment? Pathol Oncol Res. 2025;31:1612022. doi:10.3389/pore.2025.1612022.
6. Reck M, Rodríguez-Abreu D, Robinson AG, et al. Pembrolizumab versus Chemotherapy for PD-L1-Positive Non-Small-Cell Lung Cancer. N Engl J Med. 2016;375(19):1823-1833.
7. Borghaei H, Paz-Ares L, Horn L, et al. Nivolumab versus Docetaxel in Advanced Nonsquamous Non-Small-Cell Lung Cancer. N Engl J Med. 2015;373(17):1627-1639.
8. Sharma P, Allison JP. The future of immune checkpoint therapy. Science. 2015;348(6230):56-61.
9. Wu L, Yang LY, Sun J, et al. Synergistic changes in bystander CD8 and conventional CD4 T cells during neoadjuvant chemoimmunotherapy for non-small cell lung cancer reveal treatment response. Pathol Oncol Res. 2025;31:1612229. doi:10.3389/pore.2025.1612229.
10. Binnewies M, Roberts EW, Kersten K, et al. Understanding the tumor immune microenvironment (TIME) for effective therapy. Nat Med. 2018;24(5):541-550.
11. Chen DS, Mellman I. Elements of cancer immunity and the cancer-immune set point. Nature. 2017;541(7637):321-330.
12. Tumeh PC, Harview CL, Yearley JH, et al. PD-1 blockade induces responses by inhibiting adaptive immune resistance. Nature. 2014;515(7528):568-571.
13. Curiel TJ, Coukos G, Zou L, et al. Specific recruitment of regulatory T cells in ovarian carcinoma fosters immune privilege and predicts reduced survival. Nat Med. 2004;10(9):942-949.

14. Mariathasan S, Turley SJ, Nickles D, et al. TGFβ attenuates tumour response to PD-L1 blockade by contributing to exclusion of T cells. Nature. 2018;554(7693):544-548.
15. Kawano S, Ono H, Takao K, et al. Molecular cloning and characterization of a novel pyridine nucleotide-disulfide oxidoreductase family protein (*PYROXD2*) highly expressed in mouse testis. Biochem Biophys Res Commun. 2004;314(1):166-174.
16. Kwasniak M, Majewski P, Skibior R, et al. Silencing of the mitochondrial orthologue of pyridine nucleotide-disulfide oxidoreductase (*PYROXD2*) induces cell cycle arrest and apoptosis in HeLa cells via p53 and NF-κB pathways. FEBS J. 2013;280(17):4221-4236.
17. Zhang L, Li Y, Wang Q, et al. The *PYROXD2* as a potential tumor suppressor in renal cell carcinoma by inducing cell cycle arrest and apoptosis. J Cancer. 2020;11(7):1862-1872.
18. Wang H, Li H, Zhang L, et al. Overexpression of *PYROXD2* inhibits proliferation and induces apoptosis in bladder cancer cells. Oncol Rep. 2018;39(4):1635-1644.
19. Uhlen M, Fagerberg L, Hallstrom BM, et al. Proteomics. Tissue-based map of the human proteome. Science. 2015;347(6220):1260419.
20. Tang Z, Kang B, Li C, Chen T, Zhang Z. GEPIA2: an enhanced web server for large-scale expression profiling and interactive analysis. Nucleic Acids Res. 2019;47(W1):W556-W560.
21. Altorki NK, Markowitz GJ, Gao D, et al. The lung microenvironment: an important regulator of tumour growth and metastasis. Nat Rev Cancer. 2019;19(1):9-31.
22. Hegde PS, Chen DS. Top 10 Challenges in Cancer Immunotherapy. Immunity. 2020;52(1):17-35.
23. Tang H, Xiao G, Behrens C, et al. A 12-gene set predicts survival benefits from adjuvant chemotherapy in non-small cell lung cancer patients. Clin Cancer Res. 2013;19(6):1577-1586.
24. Botling J, Edlund K, Lohr M, et al. Biomarker discovery in non-small cell lung cancer: integrating gene expression profiling, tissue microarrays and immunohistochemistry. Lung Cancer. 2013;79(1):62-68.
25. Vara JÁ, Casado E, de Castro J, Cejas P, Belda-Iniesta C, González-Barón M. PI3K/Akt signalling pathway and cancer. Cancer Treat Rev. 2004;30(2):193-204.
26. Fridman WH, Zitvogel L, Sautès-Fridman C, Kroemer G. The immune contexture in cancer prognosis and treatment. Nat Rev Clin Oncol. 2017;14(12):717-734.
27. Gajewski TF, Schreiber H, Fu YX. Innate and adaptive immune cells in the tumor microenvironment. Nat Immunol. 2013;14(10):1014-1022.
28. Zaher HS, Green R. Fidelity at the molecular level: lessons from protein synthesis. Cell. 2009;136(4):746-762.
29. Ardicli D, Dincer P, Topaloglu H. A novel *PYROXD2* mutation causing congenital myopathy with rimmed vacuoles, and literature review. Neuromuscul Disord. 2021;31(10):1085-1092.
30. Ribas A, Wolchok JD. Cancer immunotherapy using checkpoint blockade. Science. 2018;359(6382):1350-1355.
31. Guillerey C, Huntington ND, Smyth MJ. Targeting natural killer cells in cancer immunotherapy. Nat Immunol. 2016;17(9):1025-1036.
32. Morvan MG, Lanier LL. NK cells and cancer: you can teach innate cells new tricks. Nat Rev Cancer. 2016;16(1):7-19.
33. Manning BD, Toker A. AKT/PKB Signaling: Navigating the Network. Cell. 2017;169(3):381-405.

34. Stahl M, Dijkers PF, Kops GJ, et al. The forkhead transcription factor FoxO regulates transcription of p27Kip1 and Bim in response to IL-2. J Immunol. 2002;168(10):5024-5031.
35. Peng SL. The T-box transcription factor T-bet in immunity and autoimmunity. Cell Mol Immunol. 2006;3(2):87-95.
36. Wendel M, Galani IE, Suri-Payer E, Cerwenka A. Natural killer cell accumulation in tumors is dependent on IFN-γ and CXCR3 ligands. Cancer Res. 2008;68(20):8437-8445.
37. Glasner A, Levi A, Enk J, et al. NKp46 Receptor-Mediated Interferon-γ Production by Natural Killer Cells Increases Fibronectin 1 to Alter Tumor Architecture and Control Metastasis. Immunity. 2018;48(1):107-119.e4.
38. Iannello A, Thompson TW, Ardolino M, Marcus A, Raulet DH. Immunosurveillance and immunotherapy of tumors by innate immune cells. Curr Opin Immunol. 2016;38:52-58.
39. Herbst RS, Soria JC, Kowanetz M, et al. Predictive correlates of response to the anti-PD-L1 antibody MPDL3280A in cancer patients. Nature. 2014;515(7528):563-567.
40. Galon J, Bruni D. Approaches to treat immune hot, altered and cold tumours with combination immunotherapies. Nat Rev Drug Discov. 2019;18(3):197-218.
41. Lanitis E, Dangaj D, Irving M, Coukos G. Mechanisms regulating T-cell infiltration and activity in solid tumors. Ann Oncol. 2017;28(suppl_12):xii18-xii32.
42. Melero I, Rouzaut A, Motz GT, Coukos G. T-cell and NK-cell infiltration into solid tumors: a key limiting factor for efficacious cancer immunotherapy. Cancer Discov. 2014;4(5):522-526.
43. Walsh NC, Kenney LL, Jangalwe S, et al. Humanized mouse models of clinical disease. Annu Rev Pathol. 2017;12:187-215.
44. Demaria O, Cornen S, Daëron M, Morel Y, Medzhitov R, Vivier E. Harnessing innate immunity in cancer therapy. Nature. 2019;574(7776):45-56.
45. Myers JA, Miller JS. Exploring the NK cell platform for cancer immunotherapy. Nat Rev Clin Oncol. 2021;18(2):85-100.
46. Hanahan D, Weinberg RA. Hallmarks of cancer: the next generation. Cell. 2011;144(5):646-674.
47. Engelman JA. Targeting PI3K signalling in cancer: opportunities, challenges and limitations. Nat Rev Cancer. 2009;9(8):550-562.
48. Janke LJ, Kim HS, O'Sullivan TE. Metabolic programming of NK cell anti-viral immunity. Curr Opin Immunol. 2021;72:1-7.
49. Marcus A, Gowen BG, Thompson TW, et al. Recognition of tumors by the innate immune system and natural killer cells. Adv Immunol. 2014;122:91-128.
50. O'Donnell JS, Teng MWL, Smyth MJ. Cancer immunoediting and resistance to T cell-based immunotherapy. Nat Rev Clin Oncol. 2019;16(3):151-167.
51. Pitt JM, Vétizou M, Daillère R, et al. Resistance Mechanisms to Immune-Checkpoint Blockade in Cancer: Tumor-Intrinsic and -Extrinsic Factors. Immunity. 2016;44(6):1255-1269.
52. Zhang Q, Bi J, Zheng X, et al. Blockade of the checkpoint receptor TIGIT prevents NK cell exhaustion and elicits potent anti-tumor immunity. Nat Immunol. 2018;19(7):723-732.

Supplementary Files

This is a list of supplementary files associated with this preprint. Click to download.

- wb.docx